Study of the $LiFePO_4/FePO_4$ Two-Phase System by High-Resolution Electron Energy Loss Spectroscopy

L. Laffont,*,† C. Delacourt,† P. Gibot,† M. Yue Wu,‡ P. Kooyman,‡ C. Masquelier,† and J. Marie Tarascon†

Université de Picardie Jules Verne, LRCS, 33 rue Saint Leu, 80039 Amiens Cedex 9, France, and National Centre for HREM, Lorentz weg 1, 2628 CJ Delft, The Netherlands

Received July 24, 2006. Revised Manuscript Received September 7, 2006

The intriguingly fast electrochemical response of the insulating $LiFePO_4$ insertion electrode toward Li is of both fundamental and practical importance. Here we present a comprehensive study of its deinsertion/insertion mechanism by high-resolution electron energy loss spectroscopy on thin platelet-type particles of Li_xFePO_4 (b_{Pnma} axis normal to the surface). We find that the lithium deinsertion/insertion process is not well-described by the classical shrinking core model. Compositions of the same x value obtained by both deinsertion and insertion gave the same results, namely that the Li_xFePO_4 so formed consists of a core of $FePO_4$ surrounded by a shell of $LiFePO_4$ with respective ratios dependent on x. We suggest that lattice mismatch between the two end members may be at the origin of the peculiar microstructure observed. Furthermore, because of the appearance of isosbestic points on the overlaid EELS spectra, we provide direct experimental evidence that the nanometer interface between single-phase areas composed of $LiFePO_4$ or $FePO_4$ is the juxtaposition of the two end members and not a solid solution. One future prospect of such knowledge is to determine strategies on how to control, on a large scale, the synthesis of nanometer-sized thin platelet-type particles to prepare high-rate $LiFePO_4$ electrodes for future energy storage devices.

Introduction

Li-ion batteries are presently enjoying the use of the layered $LiNi_{1/3}Mn_{1/3}Co_{1/3}O_2$ materials that show the highest energy density while offering some advantages over $LiCoO_2$ in terms of safety.[1] Such technology has captured the portable electronic market; however, less-expensive positive electrode materials will be required if we ever want such technology to widely penetrate the upcoming hybrid electric vehicle market. Although the spinel $LiMn_2O_4$ is being strongly considered for such large scale applications,[2] a recent leading contender that fulfills that requirement is $LiFePO_4$. Initially, the main drawbacks of this cheap and nontoxic material were both its poor electronic and ionic conductivity,[3] the reason why such an electrode material has long been disregarded. Various chemical routes to producing carbon coatings at the surface of $LiFePO_4$ particles (e.g., enhancing electronic percolating network around the particles) or aimed at decreasing particle sizes to reduce the ionic diffusion pathways have led numerous groups to elaborate highly electrochemically optimized $LiFePO_4$ powders.[4−7] Such improvements have led the A123 Company to commercialize a Li-ion $LiFePO_4$/C cell showing outstanding rate capabilities,[8] thus prevailing over 20 years of belief that insulating insertion compounds could not be used as electrode materials. Because of the practical relevance of this system and its foreseen use, it is important to understand its fundamental aspects, namely the fast electrochemical response of this poorly electronic and ionic conducting two-phase system $LiFePO_4/FePO_4$ recently described by Chen et al. as an electrochemical "miracle".[9]

This is a lively research topic that is dragging numerous research efforts and generating great debates like the importance of the ionic vs electronic conductivity,[10−12] cationic supervalent doping,[13−17] two-phase redox mechanism,[18,19−22] and interfaces (e.g., boundary interface migra-

* Corresponding author. E-mail: lydia.laffont@u-picardie.fr.
† Université de Picardie Jules Verne.
‡ National Centre for HREM.

(1) Dahn, J. R.; Fuller, E. W.; Von Sacken, U. *Solid State Ionics* **1994**, *69*, 265.
(2) Thackeray, M. M.; Johnson, P. J; De Piciotto, L. A; Bruce P. G.; Goodenough, J. B. *Mater. Res. Bull.* **1984,** *19*, 179.
(3) Delacourt, C.; Laffont, L.; Bouchet, R.; Wurm, C.; Leriche, J. B.; Morcrette, M.; Tarascon, J. M.; Masquelier, C. *J. Electrochem. Soc.* **2005**, *152* (5), A913.
(4) Yamada, A.; Chung, S. C.; Hinokuma, K. *J. Electrochem. Soc.* **2001**, *148*, A224.
(5) Audemer, A.; Wurm, C.; Morcrette, M.; Gwizdala, S.; Masquelier, C. *World Patent* 2004, WO 2004/001881 A2.
(6) Dominko, R; Goupil, J. M.; Bele, M.; Gaberscek, M.; Remskar, M.; Hanzel, D.; Jamnik, J. *J. Electrochem. Soc.* **2005**, *152*, A858.
(7) Delacourt, C.; Poizot, P.; Levasseur, S.; Masquelier, C. *Electrochem. Solid-State Lett.* **2006**, *9* (7), A352.
(8) http://www.a123systems.com/.
(9) Chen, G.; Song, X.; Richardson, T. J. *Electrochem. Solid-State Lett.* **2006**, *9* (6), A295.
(10) Morgan, D.; Ven, A. V. D.; Ceder, G. *Electrochem. Solid-State Lett.* **2004**, *7* (2), A30.
(11) Islam, S. M.; Driscoll, D. J.; Fisher, C. A. J.; Slater, P. R. *Chem. Mater.* **2005**, *17*, 5085.
(12) Maxisch, T.; Zhou, F.; Ceder, G. *Phys. Rev. B* **2006**, *73*, 104301.
(13) Chung, S. Y.; Bloking, J. T.; Chiang, Y. M. *Nat. Mater.* **2002**, *1*, 123.
(14) Chung, S.-Y.; Chiang, Y.-M. *Electrochem. Solid-State Lett.* **2003**, *6*, A278.
(15) Ravet, N.; Abouimrane, A.; Armand, M. *Nat. Mater.* **2003**, *2*, 702.
(16) Delacourt, C.; Wurm, C.; Laffont, L.; Leriche, J. B.; Masquelier, C. *Solid State Ionics* **2006**, *177*, 333.
(17) Subramanya, H. P.; Ellis, B.; Coombs, N.; Nazar, L. F. *Nat. Mater.* **2004**, *3*, 147−152.
(18) Srinivasan, V.; Newman, J. *J. Electrochem. Soc.* **2004**, *151* (10), 1517.

10.1021/cm0617182 CCC: $33.50
Published on Web 10/14/2006

tion)[9,18,19,23,24] on the Li-ion deinsertion/insertion kinetics so as to precisely simulate the electrochemical behavior of such a two-phase system.

Back in 1997, Padhi et al. suggested the shrinking core model, which simply envisages a radius-dependent process in which the $LiFePO_4/FePO_4$ interface moves inward through each particle as the outer region converts to $FePO_4$ to account for the poor capacity and rate capabilities measured earlier for $LiFePO_4$ electrodes.[24] Slight deviations from such a model were then put forward by Andersson et al., who introduced besides the radial model (e.g., the shrinking core model), the mosaic model, which considers the feasibility of the extraction/reinsertion to occur at many sites within a given particle.[23] Later on, Srinivasan et al. mathematically consolidated the shrinking core model by taking into account both the diffusion of Li through the shell and the movement of the phase boundary, and then raising the question of partial solid solution domains that are bound to exist if a radial model is assumed.[18] Searching for such $Li_{1-\epsilon}FePO_4$ and $Li_\delta FePO_4$ single-phase regions, Delacourt et al. reported the existence of solid solutions at elevated temperatures.[22] Following that track, Yamada et al. recently suggested that solid solutions could exist at room temperature, as witnessed by Rietveld refinements of X-ray and neutron diffraction data on $LiFePO_4$ nanoparticles, as well as calorimetric measurements, thus comfirming the shrinking core model.[19,20] Nevertheless, it should be realized that such a model is the result of simple logistic views or speculations. To elucidate the mechanism of how such two-phase insertion proceeds, Chen et al. studied the $LiFePO_4-FePO_4$ phase transition by high-resolution electron microscopy using micrometer platelet-like crystals.[9] They spotted the occurrence of disordered transition zones in the *bc*-plane, as the phase boundary progresses in the direction of the *a*-axis, with the Li-ions moving in a direction parallel to the phase boundary (e.g., along the *b*-direction). Although the size of the particles could have a critical bearing on the transport of Li^+ ions and electrons into and out of the individual particle, such a study has clearly shown that the well adopted core shell model does not apply to individual crystallites. In a recent report, Prosini even considered a model within which the delithiated phase grows from the center of the particle so as to reduce the stress originating from volume contraction associated with the lattice mismatch between the two end-member phases.[25]

Having succeeded in preparing nanometer-sized thin platelet-type particles through a low-temperature precipitation process,[7] we decided to further address this two-phase reaction mechanism through the use of both high-resolution transmission electron microscopy (HRTEM) coupled with high-resolution electron energy loss spectroscopy (HREELS), which is a powerful tool to study phase compositions on the nanometer scale. Our results are along the line of those of Chen et al. and further invalidate the shrinking core model, as the partially delithiated or lithiated particles are both made of a core of $FePO_4$ surrounded by a shell of $LiFePO_4$, the respective ratios of which depend on the *x* value. Furthermore, the interface was clearly shown to be the juxtaposition of the two end members rather than a solid solution.

Table 1. Global Compositions of the Chemical/Electrochemical Lithiated/Delithiated Samples[a]

type	global composition
Delithiation	
chemical	$Li_{0.26}FePO_4$
	$Li_{0.45}FePO_4$
	$Li_{0.75}FePO_4$
electrochemical	$Li_{0.5}FePO_4$
Lithiation	
chemical	$Li_{0.26}FePO_4$
electrochemical	$Li_{0.5}FePO_4$

[a] $LiFePO_4$ and $FePO_4$ were used as references.

Experimental Section

To conduct such a study, the first prerequisite was to obtain the HREELS spectra of the end members $LiFePO_4$ (LFP) and $FePO_4$ (FP) as references. $LiFePO_4$ particles with an average size of ca. 140 nm with very narrow particle size distribution were obtained from a straightforward precipitation route, as described in ref 7.[7] $LiFePO_4$ was used as a raw material for the preparation of $FePO_4$. To this end, a suspension of 400 mg of $LiFePO_4$ in a solution of NO_2BF_4 (Acrös Organics, 97%) in 20 mL of acetonitrile was stirred at RT in an environmentally controlled dry box for ca. 2 days.[26] A slight molar excess of NO_2BF_4 was used.

In order to follow the nature of $LiFePO_4/FePO_4$ system, we investigated various two-phase $xLiFePO_4/(1-x)$ $FePO_4$ samples of general formula Li_xFePO_4 by HREELS (Table 1). These partially charged or discharged samples were prepared either by chemical or electrochemical means. The electrochemical oxidation of $LiFePO_4$ or reduction of $FePO_4$ was performed in a Swagelok-type cell assembled in an environmentally controlled dry box, using Li metal as the negative electrode and a Whatman GF/D borosilicate glass fiber sheet soaked with 1 M $LiPF_6$ in 1:1 (w/w) ethylene carbonate (EC):dimethyl carbonate (DMC) as the electrolyte. A 1 cm^2, 75 μm thick composite electrode disk containing 10−15 mg of $LiFePO_4$ (for the oxidation reactions) or $FePO_4$ (for the reduction reactions) mixed with 16% of carbon ketjen black (EC-300 J, Akzo Nobel) was used as the positive electrode. The electrochemical oxidation/reduction was monitored with a VMP automatic cycling/data recording system (Biologic S.A., Claix, France), operating in galvanostatic mode at a regime of *C*/50 (1 mol of e^- exchanged in 50 h) with the final condition $\Delta x = 0.5$.

$Li_{0.26}FePO_4$ was obtained by the chemical reduction of heterosite $FePO_4$ by using an excess of LiI in acetonitrile.[27] A suspension of 100 mg of $FePO_4$ (prepared by chemical delithiation as described above) in a solution of 45 mg of LiI in 100 mL of acetonitrile was stirred for 24 h. The powder was then recovered by centrifugation and washed several times with acetonitrile in an environmentally controlled dry box.

(19) Yamada, A.; Koizumi, H.; Sonoyama, N.; Kanno, R. *Electrochem. Solid-State Lett.* **2005**, *8* (8), A409.
(20) Yamada, A.; Koizumi, H.; Nishimura, S. I.; Sonoyama, N.; Kanno, R.;Yonemura, M.; Nakamura, T.; Kobayashi, Y. *Nat. Mater.* **2006**, *5*, 357.
(21) Dodd, J.; Yazami, R.; Fultz, B. *Electrochem. Solid-State Lett.* **2006**, *9* (3), A151.
(22) Delacourt, C.; Poizot, P.; Tarascon, J. M.; Masquelier, C. *Nat. Mater.* **2005**, *4*, 254.
(23) Andersson, A. S.; Thomas, J. O. *J. Power Sources* **2001**, *97*, 498.
(24) Padhi, A. K.; Nanjundaswamy, K. S.; Goodenough, J. B. *J. Electrochem. Soc.* **1997**, *144*, A1188.
(25) Prosini, P. P. *J. Electrochem. Soc.* **2005**, *152* (10), A1925.
(26) Wizanski, A. R.; Rauch, P. E.; Disalvo, J. F. *J. Solid State Chem.* **1989**, *81*, 203.
(27) Popov, A. I.; Geske, D. H. *J. Am. Chem. Soc.* **1958**, *80*, 1340.

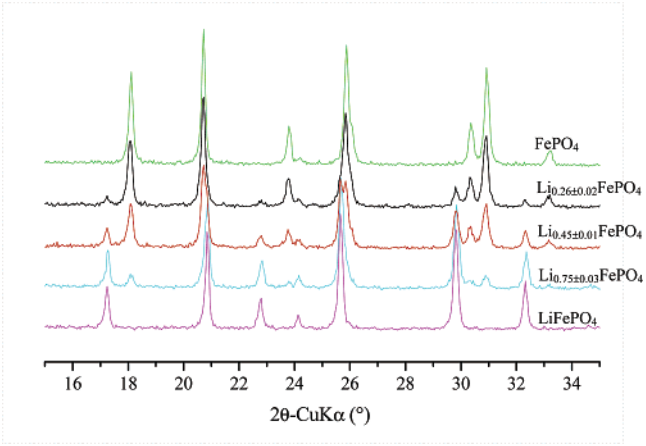

Figure 1. X-ray diffraction patterns of a series of Li_xFePO_4 compositions ($0 \leq x \leq 1$), prepared by chemical delithiation of $LiFePO_4$.

A series of Li_xFePO_4 compositions ($0 \leq x \leq 1$), prepared by chemical delithiation of $LiFePO_4$, were obtained by the same method as that described above for $FePO_4$, with x being controlled by the initial stoichiometry of NO_2BF_4 in the solution. The corresponding X-ray diffraction patterns (XRD) were collected on a Philips PW 1710 diffractometer ($\theta-2\theta$, Cu Kα radiation, back monochromator) and are shown in Figure 1. Values of x were deduced from calibration curves of the I_{LFP}:($I_{LFP} + I_{FP}$) ratios of the intensities of both (200) and (210) reflections established from XRD patterns of xLiFePO$_4$ + $(1 - x)$FePO$_4$ mixtures (prepared by simply mixing $LiFePO_4$ and $FePO_4$ powders in a mortar). Integrations and decompositions of the diffraction peaks were made using the FullProf Suite.[28]

In order to determine the nanotexture of Li_xFePO_4, we completed investigations using high-resolution transmission electron microscopy (HRTEM). Electron-transparent samples were obtained by dispersing the sample in an appropriate solvent, and one drop was subsequently deposited on copper grids coated with a lacy-carbon film. The TEM and HRTEM imaging were performed using a FEI TECNAI F20 S-TWIN. The diffraction patterns were performed using the selected area diffraction (SAED) mode or by Fourier transform of the HRTEM imaging.

For EELS analyses, the high-energy resolution spectra were recorded at the National Centre for HREM at the Delft University of Technology, The Netherlands, on a FEI TECNAI microscope operating at 200 keV with a Wien filter monochromator and equipped with an improved high tension tank and a high-resolution GIF (HR-GIF). Measurements were done at a total energy resolution of 0.25 eV, determined by measuring the full width at half-maximum of the zero-loss peak. After some tuning, the following conditions were chosen for the EEL spectra acquisition: an illumination semiangle $\alpha = 1.9$ mrad, a collection semiangle $\beta = 3.8$ mrad, and an energy dispersion of 0.05 eV/channel. The energy positions of the Fe$-L_{2,3}$ and O$-$K edges were accurately determined using the coarse internal calibration system based on the electrostatic drift tube of the EELS spectrometer. In order to follow the $LiFePO_4$/$FePO_4$ transition phase, EELS, and more specifically energy loss near edge structure (ELNES), was performed with the microscope working in the scanning transmission mode (STEM). Series of spectra were recorded by digitally scanning a STEM probe about 2 nm in diameter across the particles. All the line scans were recorded using a computer drift correction procedure integrated within the TIA software, operating every five spectra. On the basis of the energy range recorded, the spectrometer entrance aperture defining the collection efficiency was 2 mm, and the corresponding collection angles were 5.84 mrad.

(28) Rodriguez-Carvajal, J. *Physica B* **1993**, *192*, 55.

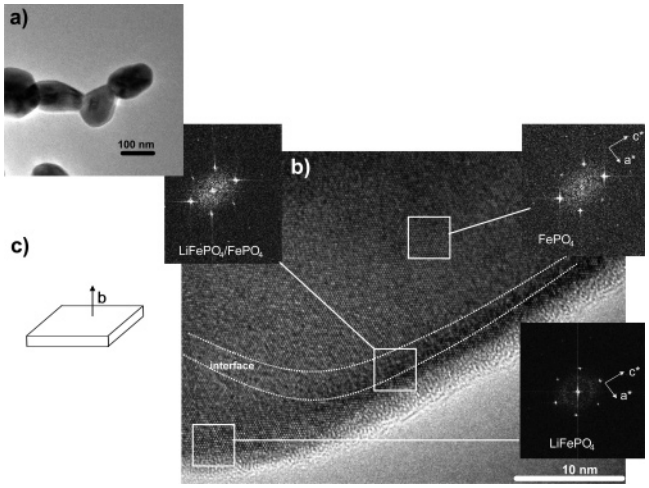

Figure 2. (a) TEM and (b) HRTEM imaging of the chemically delithiated sample of $Li_{0.45}FePO_4$. The Fourier transforms of the HRTEM imaging enable the determination of the nature of the phase present in the edge, core, or interface of the particle, respectively. (c) Sketch of the particle in this study.

Results

The HRTEM study of the two end members has also been reported in a previous paper.[7] Morphologies and nanostructures of the chemically/electrochemically delithiated/lithiated Li_xFePO_4 samples were studied by HRTEM. They have the same global morphologies as pristine $LiFePO_4$ (and $FePO_4$). Particles of the partially chemically delithiated sample of $Li_{0.45}FePO_4$ are about 200 $\times$ 100 nm^2 in size (depth of ca. 50 nm) and are very homogeneous in morphology (Figure 2a). HRTEM observations (Figure 2b) show the presence of $FePO_4$, mostly localized in the particle's core, whereas $LiFePO_4$ is present in the edge area. The peripheral area (interface highlighted in Figure 2b), in which the two phases are simultaneously present, is a transition region that is not disordered and probably supports a composition gradient that allows the two phases to coexist despite the lattice mismatch (see the HREELS part). The Fourier transform of the interface region is composed of diffraction spots for the two phases, indexed as $LiFePO_4$ and $FePO_4$. Note that both $LiFePO_4$ and $FePO_4$ have directions in common, so that the desinsertion/insertion reaction is topotactic. Moreover, for all of the delithiated/lithiated samples Li_xFePO_4, the plate-like crystals lie in the *ac*-plane with the *b*-axis perpendicular to *ac* (when $LiFePO_4$ and $FePO_4$ are indexed in *Pnma*). A particle is sketched in Figure 2c. According to Morgan,[10] and later confirmed by S. Islam,[11] $[010]_{Pnma}$ is the only direction along which the Li^+ ions can move in the $LiFePO_4$ framework. In order to follow the phase transition at the particle scale, we performed a HREELS study. The new generation of thermally assisted FEG TEM/STEM systems, equipped with a high-resolution imaging filter and a monochromator and using an energy resolution in the range of 0.2 eV, enables to study in detail the fine structures at the 3d transition metal $L_{2,3}$ edges together with the oxygen K edges. The quality of the data is similar to XAS obtained

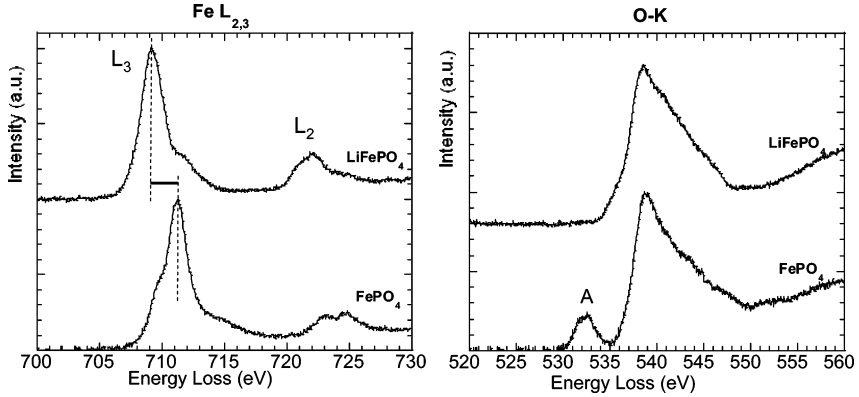

Figure 3. Fe−$L_{2,3}$ and O−K edge spectra of the reference $LiFePO_4$ and $FePO_4$.

with high-resolution monochromators.[29] This opens the exciting possibility of studying the electronic structure of materials with the same physical method either in a surface-sensitive (XAS) or in a bulk sensitive (EELS) mode, with complete geometric structure information (SAED, HREM) and a nanometer lateral resolution.

References: $LiFePO_4$ and $FePO_4$ Samples. Figure 3 shows the Fe−$L_{2,3}$ and the O−K edge spectra of $LiFePO_4$ and $FePO_4$, which can be taken as the reference spectra of $Fe^{2+}$and Fe^{3+}, respectively. Because intra-atomic correlations are pre-eminent, EELS Fe−$L_{2,3}$ edges correspond to excitations from the $2p^63d^n$ Fe ground state toward the $2p^53d^{n+1}$ Fe states (Figure 3a). The two major features of these edges are the strong white lines L_3 and L_2 due to the spin orbit splitting of the 2p core hole and separated by about 12 eV. Most fine spectral features can be clearly observed on the edge structure. $FePO_4$ (Fe^{3+} in the octahedral site) is characterized by an L_3 edge with a leading shoulder and a peak maximum at 711 eV, whereas $LiFePO_4$ (Fe^{2+} in the octahedral site) is characterized by an L_3 edge peak maximum at 709.15 eV, with no leading shoulder and a small plateau feature at ∼712 eV. The leading shoulder for $FePO_4$ and the plateau feature for $LiFePO_4$ at the Fe−L_3 edge reflect a site dependence (both in the octahedral site)[30] and not a mixing of the two structures. The collection angle for the acquisition of the EELS spectra was about 3.8 mrad, and therefore small enough to ensure that the dipole selection rule applies (the dipole selection rule is valid for $qr \gg 1$, where q is the momentum transfer and r the average radius of the overlap between the initial and final states[31]). Meanwhile, chemical shifts of 1.85 eV have been measured, at the maximum of the Fe−L_3 line, between the two oxidation states (Fe^{2+} and Fe^{3+}), respectively. These Fe−$L_{2,3}$ edges show a characteristic behavior with changing Fe valence state.

The O−K edge in $LiFePO_4$ and $FePO_4$ (Figure 3b) is due to an excitation of the 1s orbital to unoccupied O 2p orbitals. Phosphate minerals containing octahedral Fe^{3+} show a clear initial peak A, whereas those with Fe^{2+} bonded to oxygen tend to lack this feature. This is due to a combination of the 3d orbitals of these d-block elements being too high in energy to hybridize easily with the unoccupied O 2p orbitals and the Fe^{2+} having fewer empty d-states available for hybridization as compared with Fe^{3+}.[32] The A peak is characteristic of the hybridization of iron in $FePO_4$ and is a good indicator of iron valence state in $LiFePO_4/FePO_4$.

Delithiated/Lithiated Li_xFePO_4 Samples. In order to visualize the particles, scanning transmission electron microscope (STEM) high-angle annular dark field (HAADF) imaging was used because it offers the advantage of an incoherent signal (to avoid unwanted Fresnel effects) and an increased atomic number contrast. A uniform contrast on the HAADF STEM image of a particle will also be consistent with a constant thickness of the latter. A combination of STEM and HREELS techniques will enable us to probe the chemical and valence states along the particle on the nanometer scale. Several core-line spectra (with both Fe−$L_{2,3}$ and O−K edges) were recorded across a chemically delithiated particle of global composition $Li_{0.45}FePO_4$ and size 172 nm. This scan is composed of 50 spectra corresponding to a maximum total acquisition time of 4 min in order to minimize contamination as well as irradiation and instability effects. As depicted in Figure 4, the evolution of the O−K edges and Fe−$L_{2,3}$ fine structures from one spectrum to another indicates that the particle's core is mainly composed of $FePO_4$, whereas the edge is formed of $LiFePO_4$. By following the A peak of the O−K edge at each position of the nanometer probe in Figure 4, we can easily determine the localization of the $FePO_4$ and $LiFePO_4$ phase in the particle. In order to clearly characterize the interface and show the important variations between the energy positions and the shape of Fe−$L_{2,3}$ fine structures and O−K edges along the line scan, we extracted EEL spectra characteristic of pure $LiFePO_4$, the interface between $LiFePO_4$ and $FePO_4$, and pure $FePO_4$ from the line spectra of Figure 4. We have focused on one interface of the line spectra, and the Fe−$L_{2,3}$ and O−K spectra extracted are represented in Figure 5. For the Fe−$L_{2,3}$ edges, in the interface area, the L_3 lines are clearly composed of two main peaks that roughly correspond to the contribution of the ferrous and ferric iron ions. To achieve a more quantitative determination of the redox state, we have linearly decomposed the interfacial Fe−$L_{2,3}$ edges

(29) Laffont, L.; Wu, M. Y.; Chevallier, P.; Poizot, P.; Mocrette, M.; Tarascon J. M. *Micron* **2006**, *37*, 459.
(30) Paterson, H.; Krivanek, O. L. *Ultramicroscopy* **1990**, *32*, 319.
(31) Egerton, R. F. *Electron Energy Loss Spectroscopy in the Electron Microscope*; Plenum Press: New York, 1996; Chapter 2, p 27.
(32) Calvert, C. C.; Brown, A.; Brydson, R. *J. Electron Spectra Related Phenom.* **2005**, *143*, 173.

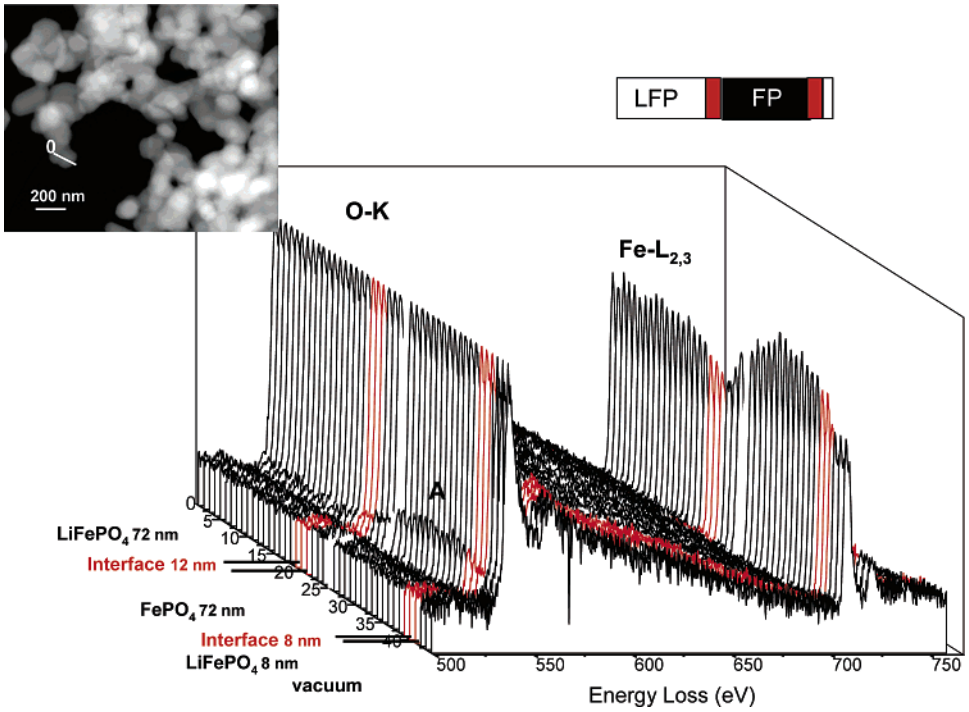

Figure 4. STEM HAADF image of the chemically delithiated sample $Li_{0.45}FePO_4$ with the analysis line and the 3D representation of EELS spectra recorded along that line. Note that the EELS spectra of the interface are represented in red.

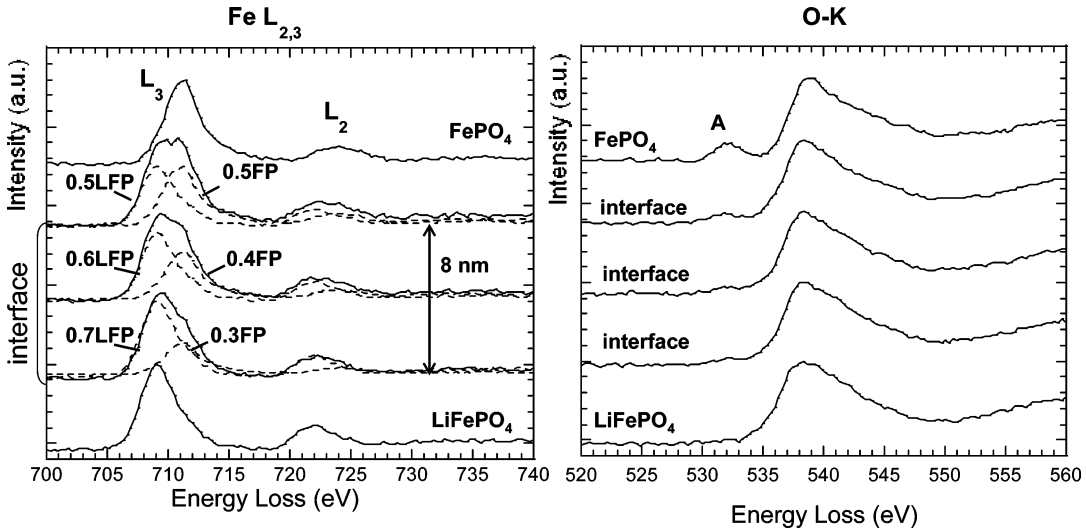

Figure 5. Focus on one interface of Figure 4. Fe−$L_{2,3}$ and O−K edge spectra of $LiFePO_4$, interface, and $FePO_4$. Spectra in dashed line represent the proportion of the two end members that enable the fit to the experimental EELS spectra of the interface.

using Fe−$L_{2,3}$ reference spectra of both $LiFePO_4$ and $FePO_4$. These two spectra are also gathered in Figure 5 and correspond to references of pure Fe^{3+} and Fe^{2+}, respectively. One observes that all of the fine structures present in the interfacial spectra can be reconstructed by a linear combination of the two references $LiFePO_4$ and $FePO_4$. The proportions of the two end members are represented by a dashed line in Figure 5. Moreover, for the O−K edge at the interface, the A peak is visible when the proportion of $FePO_4$ is superior or equal to that of $LiFePO_4$. In order to better account for the biphasic character of the interface, we have also superimposed the Fe−$L_{2,3}$ edge spectra of the interface on that of the two end members (Figure 6). Two common points (isosbestic points) are observed that are characteristic of the biphasic nature of the interface. These isosbestic points indicate that the EELS signal in the mathematical point of view is constituted of the linear combination of two contributions. In XAS spectra (close to EELS with monochromator), the existence of such isosbestic points is the hallmark of two compounds present in the mixture[33] and has also been pointed out in the deinsertion/insertion of lithium ions in the $LiFePO_4$ compound,[34] whereas the lack of this point is characteristic of a monophase and has been experimentally observed in layered substituted oxides.[35−38]

(33) Wang, X.; Hanson, J. C.; Frenkel, A. I.; Kim, J. Y.; Rodriguez, J. A. *J. Phys. Chem. B* **2004**, *108*, 13667−13673.
(34) Jain, G.; Balasubramanian, M.; Yang, J.; Xu, J. J. Private communication, **2005**.
(35) Nakai, I.; Nakagone, T. *Electrochem. Solid-State Lett.* **1998**, *1* (6), 259.

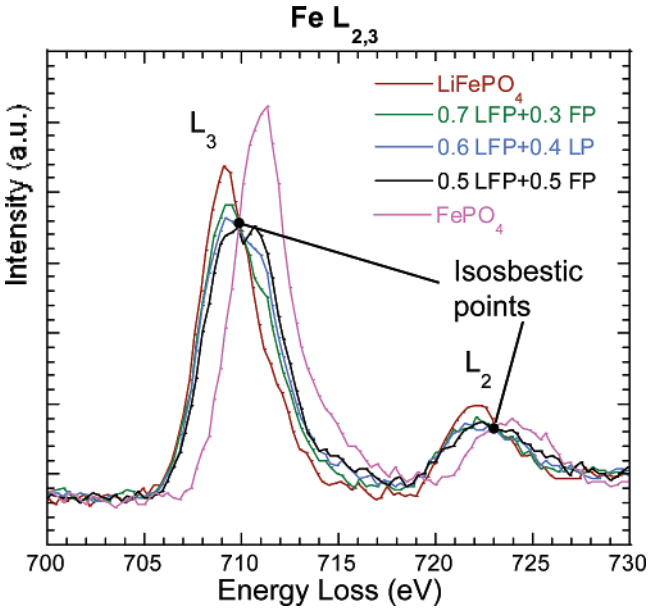

Figure 6. Superposition of the Fe−$L_{2,3}$ edge spectra of the same interface of Figure 5. Two isosbestic points are represented, which are characteristic of the biphasic nature of the interface.

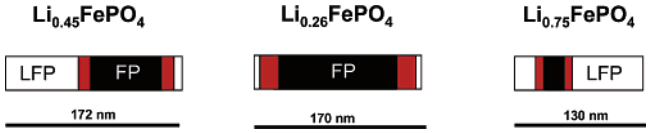

Figure 7. Schematic representation of the $Li_{0.26}FePO_4$, $Li_{0.45}FePO_4$, and $Li_{0.75}FePO_4$ particles obtained by chemical delithiation of $LiFePO_4$. Three colors were used in these sketches: white for $LiFePO_4$, black for $FePO_4$, and red for the interface.

STEM/EELS analyses allow for the localization of $LiFePO_4$ and $FePO_4$ within the particles as well as for their proportions to be determined. Moreover, STEM and HRTEM imaging enables us to determine the dimension and depth of the platelet-type particles. It is thus possible to quantify the global proportions of $LiFePO_4$ and $FePO_4$ and then to estimate the x value (which should be close to 0.45), assuming the delithiation is uniform over all of the particles. These spectra clearly indicate that the shell of the particles is composed of $LiFePO_4$ and the core of $FePO_4$ for olivine-type materials prepared by partial oxidation. The line EELS/STEM spectra have also been done in the same particle along a perpendicular direction and for other particles; the sketch for this delithiated olivine-type system is gathered as an insert in Figure 4 and in Figure 7. The same behavior was observed through STEM/EELS analyses for two other partially delithiated materials with global compositions of $Li_{0.26}FePO_4$ and $Li_{0.75}FePO_4$ (not shown here). For $Li_{0.26}FePO_4$, the sketch in Figure 7 deduced from the EELS study shows that the proportion of $FePO_4$ in the core is relatively more important than for $Li_{0.45}FePO_4$, with only a narrow edge of ca. 4 nm composed of $LiFePO_4$. For the $Li_{0.75}FePO_4$ sample, a small proportion of $FePO_4$ has been localized not in the center of the particle but rather in a corner, with all other parts being composed of $LiFePO_4$ except the interfaces (highlighted in Figure 7), which are a linear combination of the two end members. The sketch of the $Li_{0.75}FePO_4$ delithiated sample is represented in Figure 7 and determined by the STEM/EELS study. We have also investigated electrochemically delithiated samples by STEM/EELS. The same model as for the chemically delithiated samples was found (core, $FePO_4$; edge, $LiFePO_4$).

As it is interesting to know whether the model is the same or not for chemically and electrochemically lithiated samples, several core-line spectra (with both Fe−$L_{2,3}$ and O−K edges) were recorded on a chemically lithiated sample of global composition $Li_{0.26}FePO_4$. A line scan composed of 50 spectra (5 s acquisition time per spectra) is represented in Figure 8. The evolution of the O−K edges and Fe−$L_{2,3}$ fine structures from one spectrum to another indicates that the nanoparticle shell is composed of $LiFePO_4$, whereas one part, near the center of the particle, is composed of $FePO_4$. By following the A peak of the O−K edge at each position of the nanometer probe in Figure 8, the localization of the $FePO_4$ and $LiFePO_4$ phases in the particle can be easily determined. Moreover, as the particle has an important proportion of $FePO_4$ in the interface regions, the A peak is clearly present along them. In order to clearly show the important variations between the energy positions and the shape of Fe−$L_{2,3}$ fine structures and O−K edges along the line scan, EEL spectra characteristic of $LiFePO_4$, the interface between $LiFePO_4$ and $FePO_4$, and $FePO_4$ were extracted (the result of a zoom on one interface is shown in Figure 9). The same procedure to fit the experimental data by the two end-member EEL spectra have been used for the interface region. The interface is composed of a linear combination of $LiFePO_4$ and $FePO_4$ (Figure 9). The same EELS experiment has been carried out on the electrochemical lithiated sample ($Li_{0.5}FePO_4$; not shown here). The conclusion is the same (edge, $LiFePO_4$; core, $FePO_4$), with the proportion of these two phases according to the value of x in Li_xFePO_4.

Discussion

The results of our HREELS measurements on Li_xFePO_4 samples (partially delithiated and lithiated) seem at first to invalidate the classical view of insertion/deinsertion model based on the simple shrinking core with the delithiated phase domain moving in toward the particle as the lithium is removed. However, although experiments that defeat intuitive beliefs are always exciting, spurring new thoughts or new mechanisms, caution has to be exercised so as to ascertain that what is observed is not due to experimental flaws but rather reflects the intrinsic property of the material. Whatever the samples investigated, $Li_{0.26}FePO_4$, $Li_{0.45}FePO_4$, or $Li_{0.75}FePO_4$, obtained by either chemical/electrochemical delithiation or by chemical/electrochemical lithiation, we always observed from the EELS scan lines spectra particles with $FePO_4$ as the core and $LiFePO_4$ as the shell. As expected, the largest $FePO_4$ core was observed for samples with lower global lithium content. At this point, a legitimate question is whether we could have Li displacements out from the particle driven by beam heating, thus leading to the observed

(36) Balasubramanian, M.; Sun, X.; Yang, X. Q.; McBreen, J. *J. Electrochem. Soc.* **2000**, *147* (8), A2903.
(37) Yoon, W. S.; Grey, C. P.; Balasubramanian, M.; Yang, X. Q.; McBreen, J. *J. Chem. Mater.* **2003**, *15*, 3161.
(38) Jain, G.; Yang, J. C.; Balasubramanian, M.; Xu, J. J. *J. Chem. Mater.* **2005**, *17*, 3850.

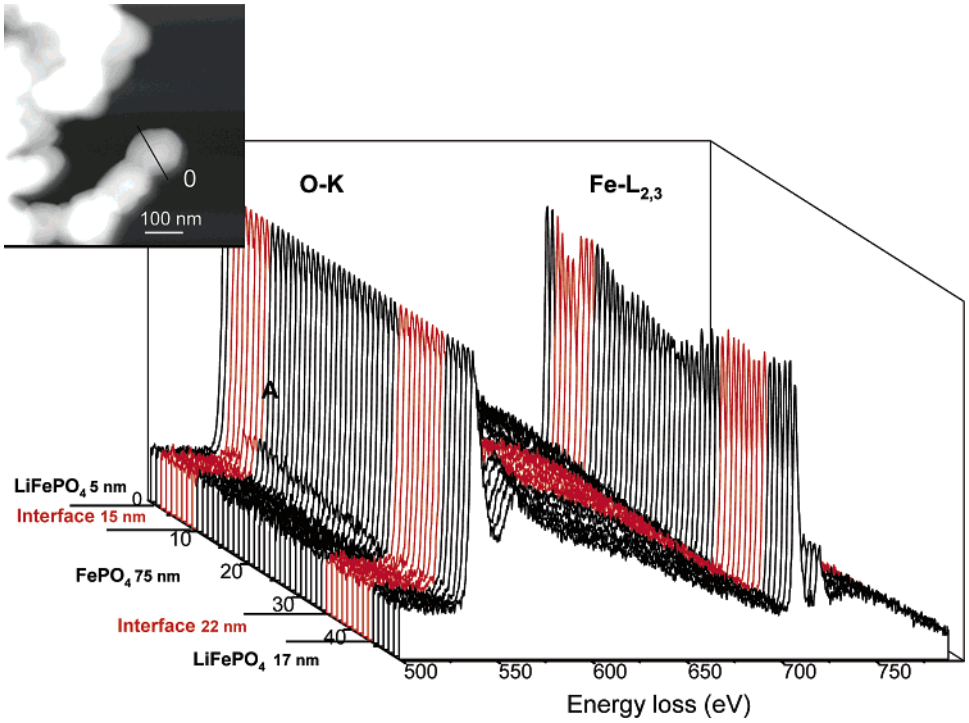

Figure 8. STEM HAADF image of the chemically lithiated sample $Li_{0.26}FePO_4$ with the analysis line and the 3D representation of EELS spectra recorded along that line. Note that the EELS spectra of the interface are represented in red.

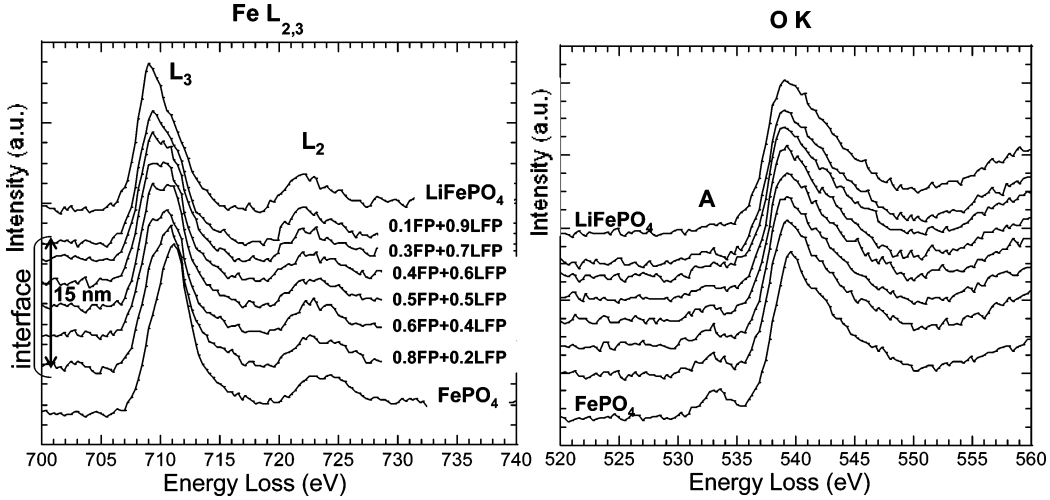

Figure 9. Focus on one interface of Figure 8. Fe−$L_{2,3}$ and O−K edge spectra of $LiFePO_4$, interface, and $FePO_4$.

configuration. This seems quite unlikely, because the material appeared stable under the beam even when either the applied voltage or exposure time was increased. Furthermore, assuming an e-beam heating effect during the recording scan line spectra, one could expect, by similarity to zone melting purification, particles with asymmetric Li distribution (e.g., opposite edges having 0 and 100% Li content), as opposed to particles having a core/shell type Li repartition, as observed here.

Let us see how we can rationalize such finding on the basis of structural consideration by first recalling the common view of the lithium extraction/insertion process. A core−shell model, with a shell of $FePO_4$ growing over a shrinking core of $LiFePO_4$ during charge and the reverse situation during discharge, has been presented up to now.[18,19,23] To account for this mechanism, we have to consider partial solid solutions of formula $Li_{1-\epsilon}FePO_4$ and $Li_\delta FePO_4$.[18,19] Upon charge or subsequent discharge, the driving force for lithium motion across either the Li-poor phase $Li_\delta FePO_4$ or Li-rich phase $Li_{1-\epsilon}FePO_4$ is the Li^+-concentration gradient within these phases. It has to be recalled, however, that this concept of a core−shell model was never experimentally evidenced for this olivine-type system.

A first limitation of this model is that it does not take into account any anisotropy arising from the fact that ion (and electron) motion is constrained by the olivine-type structure itself. Let us recall that the olivine-type structure is described in the *Pnma* space group and can be viewed as a distorted hexagonal compact structure, in which $TeOc_2$ layers are stacked perpendicularly to the *c*-direction. Fe and Li occupy one-half of the available octahedral sites and are distributed over two different crystallographic sites. Phosphorus atoms occupy 1/8 of the tetrahedral sites. The *b* parameter of the orthorhombic structure corresponds to two times the *a*′

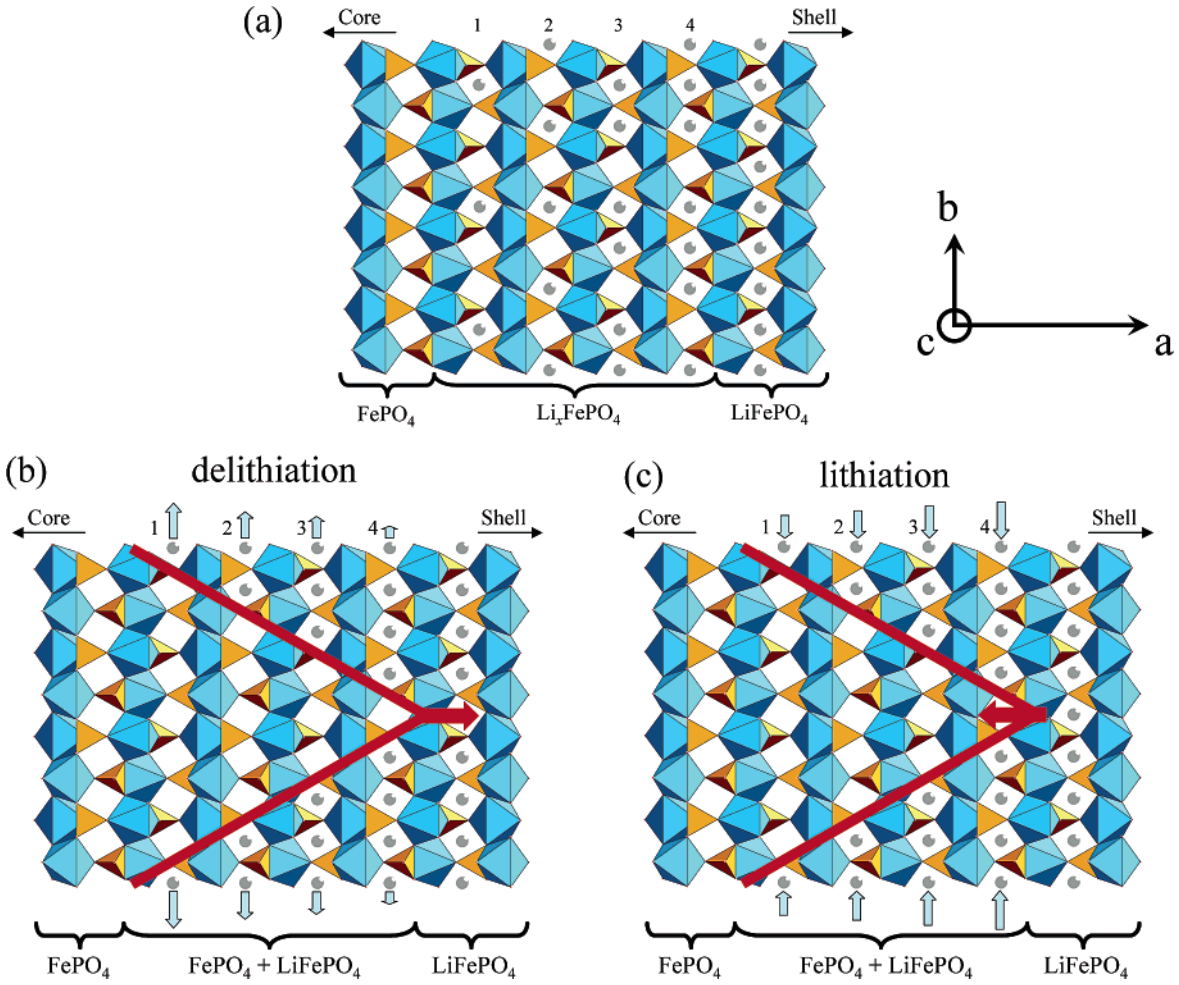

Figure 10. Schematic views of the interfacial region between $LiFePO_4$ and $FePO_4$ phases. (a) Hypothesis of a disordered Li_xFePO4 phase with a gradient of Li content between $FePO_4$ and $LiFePO_4$ end members, which is not verified by HREELS measurements; (b) front phase evolution during delithiation, deduced from HREELS; (c) front phase evolution during lithiation, deduced from HREELS. Small vertical arrows indicates the movement of (Li^+, e^-) pairs, the longest ones symbolizing an energetically favored extraction/insertion from/into the channels. The large red arrows indicate the direction in which the interfacial region is moving. Note that (i) similar sketches could be made in every plane containing the *b*-axis; (ii) the difference in lattice parameters of $LiFePO_4$ and $FePO_4$ is not taken into account in those schemes; and (iii) the number of $LiFePO_4$ (or $FePO_4$) unit cells within a particle has been reduced to about ten for clarity (the actual number of Li^+ ions within one channel is ~160−170)

parameter of the distorted hc structure and *c* corresponds to *c*′. Theoretical calculations have shown that Li motion within this structure was likely to occur only along the *b*-direction.[10,11] At first sight, a radial model also appears very unlikely, considering this 1D ionic conductivity.

A second limitation of this model is that it implies the consideration of partial solid solutions, for which the lithium solubilities (i.e., ϵ and δ values) and even the existence itself are still controversial.[18,19−22]

The shrinking core model cannot account for the observed behavior from HRTEM and HREELS measurements, especially because the two main properties of a shrinking core model detailed above are not fulfilled. Indeed, the simultaneous presence of some areas of the platelet-like particles composed only of $FePO_4$ and $LiFePO_4$ unambiguously shows that Li^+ extraction occurs by a progressive emptying of the Li channels (oriented along the *b*-axis, perpendicular to the *ac*-plane in which the particles are laid). Upon lithiation, the empty channels are progressively filled.

In between the single-phase areas composed of $LiFePO_4$ or $FePO_4$, intermediate zones composed of both end members were clearly identified by the appearance of isosbestic points on the overlaid EELS spectra. We can also invalidate a simple view of the interfacial region, which would consist of a solid solution Li_xFePO_4 with a gradient of *x* ranging from 0 to 1 by moving from $FePO_4$ to $LiFePO_4$ (schematized in Figure 10a). This result somehow entertains the controversy of the existence of the partial solid solutions domains, because even on the nanometer scale, only the two end members could be identified.

On the basis of the two main experimental observations described above, a mechanism may be proposed and is sketched in panels b and c of Figure 10 for delithiation and lithiation, respectively. As the electrons are likely to be strongly correlated to the Li^+ ions in the form of exciton-like quasiparticles ($Li_{Li}\bullet$, e_{Fe}'), as envisaged by the recent publication of Maxisch et al.,[12] we will suppose later that Li^+ ions and electrons can be seen as pairs. Let us imagine a platelet-like particle of $LiFePO_4$ laid perpendicular to the *b*-axis. The removal of one (Li^+, e^-) pair, together with the hopping of other (Li^+, e^-) pairs from the inside to the outside of the channel, will occur in the Li^+ channel where it is the most energetically favored. The further (Li^+, e^-) pairs to be removed will be subjected to two key parameters arising from

the number of (Li^+, e^-) pairs displaced by hopping (from the inward to the outward of the Li^+-channels) and the energy gain due to the proximity of a $FePO_4$ nucleus.

As shown in Figure 10b, the (Li^+, e^-) pair in channel #1 is the most likely to be removed, because of the vicinity of $FePO_4$ as well as the small numbers of (Li^+,e^-) pairs to hop. The consequence is that the front phase (interface between $LiFePO_4$ and $FePO_4$) will spread from a $FePO_4$ nucleus to the whole particle. We speculate that the $FePO_4$ nucleus is most likely to be formed near the center of the particle rather than at the periphery because of the differences between $LiFePO_4$ and $FePO_4$ unit-cell volumes (291.04 $Å^3$ for $LiFePO_4$ compared to 273.00 $Å^3$ for $FePO_4$[39]). This volume variation is anisotropic: *a* and *b* decrease by 5.0 and 3.7%, respectively, from $LiFePO_4$ to $FePO_4$, whereas *c* increases by 1.9%. Upon lithium removal from $LiFePO_4$, this corresponds to a shrinkage into the direction of the $TeOc_2$ layers (in the *ab*-plane) together with a slight increase between the layers (*c*-axis). Because of the topotactic nature of the two-phase process, the phase having the smaller unit-cell volume would be more likely to be located in the core of the particles rather than at the periphery, as also suggested by Prosini.[25] This would explain why $FePO_4$ is always found in the particle's core, whereas $LiFePO_4$ is found in the shell of the partially delithiated particles.

Upon lithiation, the scheme of Figure 10c has to be considered. This time, the nucleation of $LiFePO_4$ occurs preferentially at the periphery of the grain, for the same reason mentioned above ($LiFePO_4$ having a higher unit-cell volume than $FePO_4$). However, on the contrary, with the mechanism of delithiation, the insertion of Li^+ ions into the channels will be dependent on two competing phenomena: the number of (Li^+, e^-) pairs displaced by hopping (from the outside to the inside of the Li^+ channels) and the energy gain due to the vicinity of $LiFePO_4$ nuclei

The first effect tends to fill in the shortest and/or emptiest channels first, but according to the experimental results, this effect is mostly countered by the second one, which tends to energetically promote the insertion of Li^+ ions in the channels that are closer to $LiFePO_4$ phase (channel 4 in Figure 10c). We should also expect (i) the interfacial regions to be larger upon lithiation than upon delithiation, and (ii) the kinetics of lithiation to be more limited than that of delithiation, which has been experimentally observed through the dissymmetry reported between charge and discharge electrochemical properties (higher overpotential upon discharge than upon charge).[40]

The mechanism described here is also mostly consistent with the experimental results of the HRTEM study recently published by Chen et al.[9] However, a main difference lies in the fact that the interfacial region between $LiFePO_4$ and $FePO_4$ (likely to be composed of $LiFePO_4$ and $FePO_4$, and identified as a disordered phase by the authors) is mainly observed along the *bc*-plane of the $4 \times 2\ \mu m^2$ platelets (lying perpendicular to *b*-axis), where some dislocations exist because of the mismatch between $LiFePO_4$ and $FePO_4$ unit cells. In some cases, the authors could also identify different regions of $FePO_4$ nucleation, then leading to some cracks in the crystal because of the stress generated by lattice mismatches. We speculate that, on the contrary, highly divided powders such as those studied here do not exhibit such defaults, because they can accommodate the stress ensured by the lattice mismatch between $LiFePO_4$ and $FePO_4$ due to a nucleation of $FePO_4$ occurring mostly in the core. Of course, the lack of cracks and faults is likely to act positively toward the electrochemical performances of this material, as attested by the recent results published in ref 7.[7]

As suggested by Chen et al.,[9] these new insights about the mechanism of $LiFePO_4/FePO_4$ allow us to stress that, as Li ions move parallel to the *b*-axis, reducing the crystal size along the *b*-axis should contribute to an enhancement of the electrochemical properties of the material toward Li^+ extraction/insertion. Nevertheless, the other two dimensions of the particles should not be ignored, because besides eventually reducing the number of cracks and dislocations within the grain as we speculated above, decreasing the size of the particles in the *ac*-plane will have an impact on the electronic percolation within the electrode material. Although a carbon-nanocoating on the *ac*-faces of the crystal will certainly be required to achieve good electrochemical performances of large $LiFePO_4$ platelets (by providing an increased number of nucleation sites for $FePO_4$ during charge, according to Chen et al.[9]), thin platelet nanoparticles of $LiFePO_4$ exhibit outstanding rate capabilities without any need for carbon nanopainting (e.g., having a higher tapping density). This result is of great importance for the implementation of $LiFePO_4$ in future energy storage devices such as HEV.

Finally, we should point out that such results are not specific to $LiFePO_4$, because our HREELS studies on $LiMnPO_4$ reveal similar results: $MnPO_4$ is found in the core of the particles and $LiMnPO_4$ on the edge. It is thus quite surprising that $LiMnPO_4$ could not be easily and fully delithiated. Li^+ and e^- transport is so hindered within this material that the removal of (Li^+, e^-) pairs among some Li^+ channels (e.g., the longest ones and/or those containing defaults) will not be possible, even by chemical delithiation for which an ideal electronic percolation is mimicked through the uniform presence of the oxidant specie (NO_2^+ for instance) around the particles.

Conclusions

A combination of STEM and HREELS techniques enabled us to study the $LiFePO_4/FePO_4$ two-phase system by probing the chemical and valence state along the particles on the nanometer scale. We found that the lithium reactivity mechanism in Li_xFePO_4 cannot be described by the classical shrinking core model. Whatever the material being charged (or discharged), the phase transition occurs by a successive emptying (or filling) of the Li^+ channels (along the *b*-axis), leading to partially delithiated (or lithiated) particles both made of a core of $FePO_4$ surrounded by a shell of $LiFePO_4$. Through the use of EELS in a line scan mode, we clearly show that the nanometer interface between the single-phase

(39) Delacourt, C.; Rodriguez-Carvajal, J.; Schmitt, B.; Tarascon, J. M.; Masquelier, C. *Solid State Sci.* **2005**, *7* (12), 1506.
(40) Srinivasan, V.; Newman, J. *Electrochem. Solid-State Lett.* **2006**, *9* (3), A110.

areas composed of $LiFePO_4$ or $FePO_4$ is the superposition of these two end members rather than a solid solution. Because of the fact that our HREELS measurements were not done in situ, those willing to entertain further the single phase vs two phases controversy can still argue that we could have at the interface a short-lived solid solution region that is disproportionate to the observed products. Although such measurements cannot be presently done in situ, we hope such a work to convey the message that HREELS is becoming an increasingly powerful characterization tool for the battery community to study particles and interfaces on the nanometer scale.

Acknowledgment. We thank ALISTORE for making study available through the microscopy platform, which hosts a microscope with an HREELS.

CM0617182